Specific Interactions Measured by AFM on Living Cells between Peroxiredoxin-5 and TLR4: Relevance for Mechanis....

Article *in* Cell Chemical Biology · March 2018

DOI: 10.1016/j.chembiol.2018.02.006

7 authors, including:

Bernard Knoops
Université Catholique de Louvain
105 PUBLICATIONS **2,797** CITATIONS
SEE PROFILE

Sarah Becker
Université Catholique de Louvain
4 PUBLICATIONS **29** CITATIONS
SEE PROFILE

Mégane Poncin
Université Catholique de Louvain
2 PUBLICATIONS **0** CITATIONS
SEE PROFILE

Julien Glibert
Université Catholique de Louvain
2 PUBLICATIONS **0** CITATIONS
SEE PROFILE

Article

Cell Chemical Biology

Specific Interactions Measured by AFM on Living Cells between Peroxiredoxin-5 and TLR4: Relevance for Mechanisms of Innate Immunity

Graphical Abstract

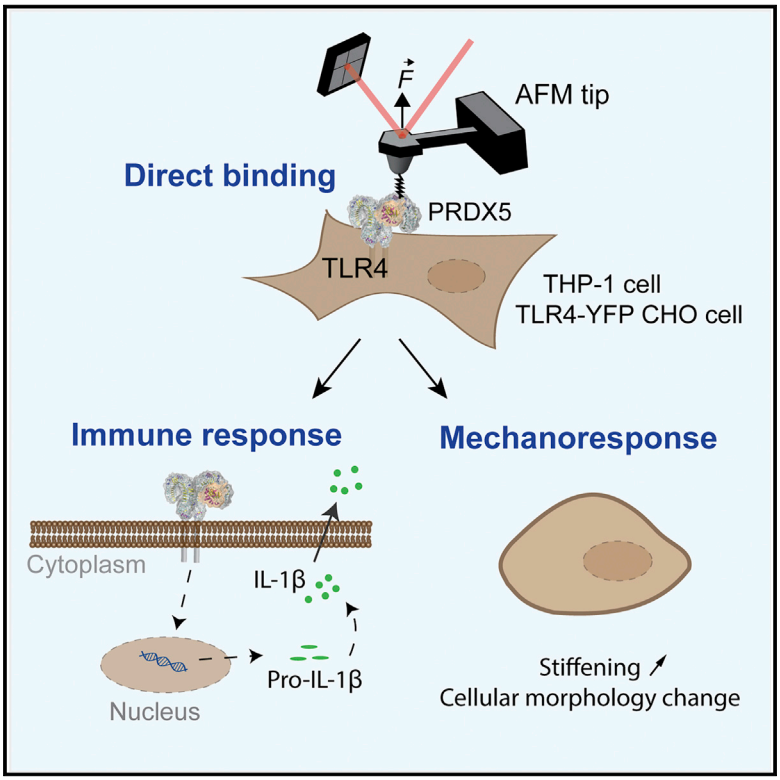

Authors

Bernard Knoops, Sarah Becker, Mégane Anne Poncin, Julien Glibert, Sylvie Derclaye, André Clippe, David Alsteens

Correspondence

bernard.knoops@uclouvain.be (B.K.), david.alsteens@uclouvain.be (D.A.)

In Brief

Knoops et al. used force-distance curve-based atomic force microscopy to investigate the molecular mechanisms by which extracellular human PRDX5 can activate a proinflammatory response. Single-molecule experiments demonstrate specific binding of PRDX5 to TLR4 on purified receptors and living cells.

Highlights

- Single-molecule experiments demonstrate that PRDX5 specifically binds to TLR4
- Specific interaction observed on THP-1 cells and CHO cells overexpressing TLR4-YFP
- PRDX5 binding induces a cellular mechanoresponse

Knoops et al., 2018, Cell Chemical Biology *25*, 1–10
May 17, 2018
https://doi.org/10.1016/j.chembiol.2018.02.006

CellPress

Please cite this article in press as: Knoops et al., Specific Interactions Measured by AFM on Living Cells between Peroxiredoxin-5 and TLR4: Relevance for Mechanisms of Innate Immunity, Cell Chemical Biology (2018), https://doi.org/10.1016/j.chembiol.2018.02.006

Cell Chemical Biology
Article

Specific Interactions Measured by AFM on Living Cells between Peroxiredoxin-5 and TLR4: Relevance for Mechanisms of Innate Immunity

Bernard Knoops,[1,*] Sarah Becker,[1] Mégane Anne Poncin,[1] Julien Glibert,[1] Sylvie Derclaye,[1] André Clippe,[1] and David Alsteens[1,2,*]
[1]Université catholique de Louvain, Institut des Sciences de la Vie (ISV), 1348 Louvain-la-Neuve, Belgium
[2]Lead Contact
*Correspondence: bernard.knoops@uclouvain.be (B.K.), david.alsteens@uclouvain.be (D.A.)
https://doi.org/10.1016/j.chembiol.2018.02.006

SUMMARY

Inflammation is a pathophysiological response of innate immunity to infection or tissue damage. This response is among others triggered by factors released by damaged or dying cells, termed damage-associated molecular pattern (DAMP) molecules that act as danger signals. DAMPs interact with pattern recognition receptors (PRRs) to contribute to the induction of inflammation. However, how released peroxiredoxins (PRDXs) are able to activate PRRs, such as Toll-like receptors (TLRs), remains elusive. Here, we used force-distance curve-based atomic force microscopy to investigate the molecular mechanisms by which extracellular human PRDX5 can activate a proinflammatory response. Single-molecule experiments demonstrated that PRDX5 binds to purified TLR4 receptors, on macrophage-differentiated THP-1 cells, and on human TLR4-transfected CHO cells. These findings suggest that extracellular PRDX5 can specifically trigger a proinflammatory response. Moreover, our work also revealed that PRDX5 binding induces a cellular mechanoresponse. Collectively, this study provides insights into the role of extracellular PRDX5 in innate immunity.

INTRODUCTION

Inflammation is an essential component of the innate immune response to infection or tissue damage, which has the physiological role of restoring tissue homeostasis. Inflammation is initiated and perpetuated by pathogen-associated molecular pattern (PAMP) and damage-associated molecular pattern (DAMP) molecules. While PAMPs are derived products of pathogens, DAMPs are host-derived nuclear or cytosolic proteins with defined intracellular functions. Following tissue injury, DAMPs are released extracellularly and move from a reducing to an oxidizing milieu. PAMPs and DAMPs are recognized by membrane-bound pattern recognition receptors (PRRs), including Toll-like receptors (TLRs), the NOD-like receptors, and RIG-I-like receptors. So, PRRs are activated and promote intracellular cascades that lead to an inflammatory response (Chen and Nunez, 2010; Kono and Rock, 2008; Kumar et al., 2013).

The superfamily of peroxidases named peroxiredoxins (PRDXs), has been reported to play important roles in innate immunity (for reviews, see Ishii et al., 2012; Knoops et al., 2016; Park et al., 2016). PRDXs are a family of thiol-dependent peroxidases that are able to reduce peroxides (hydrogen peroxide, alkyl hydroperoxides, and peroxynitrite) and are constitutively expressed by virtually all cell types in mammals (Perkins et al., 2015). It has been reported that, intracellularly, PRDXs may act as cytoprotective antioxidant enzymes, protein chaperones, modulators of peroxide signaling, and redox relays (Rhee and Kil, 2017). Interestingly, PRDXs were also shown to play a role in immune modulation as PAMPs or DAMPs upon their release into the extracellular milieu (Riddell et al., 2010b; Robinson et al., 2010; Shichita et al., 2012). Studies conducted either after brain injury in rats (Chou et al., 2011) or after acute ischemic stroke in humans (Dayon et al., 2011), demonstrated that PRDXs are released into extracellular fluids and could function as DAMPs under conditions of sterile inflammation. Moreover, Shichita et al. (2012) have shown that post-ischemic brain inflammation can be mediated through PRDXs and is dependent on TLR2 and TLR4. In particular, it was shown that, among PRDXs, PRDX5 highly contributed to induce the expression and the release of inflammatory cytokines (Shichita et al., 2012). However, the molecular mechanisms underlying TLR2 and TLR4 activation through PRDXs still remained to be clarified (Figure 1A).

Atomic force microscopy (AFM), invented to image the topography of samples at high resolution and in native conditions (Binnig et al., 1986), evolved rapidly allowing the investigation of living mammalian cells and the probing of specific interactions under physiological conditions (Alsteens et al., 2017a; Dufrene et al., 2017). Force-distance curve-based AFM (FD-based AFM) enables us to contour the surface of biological systems with simultaneous mapping of their physical properties at (sub-) nanometer resolution (Dufrene et al., 2013). A tip positioned at the very end of a soft cantilever is oscillated and scanned across a cell while performing a single approach and retract movement at each discrete point of the surface. During the approach and retraction cycle, the tip interacts with the cell surface and is deflected depending on the force exerted on it, which in turn deviates the path of a laser, reflected from the cantilever onto a position-sensitive detector. This deflection

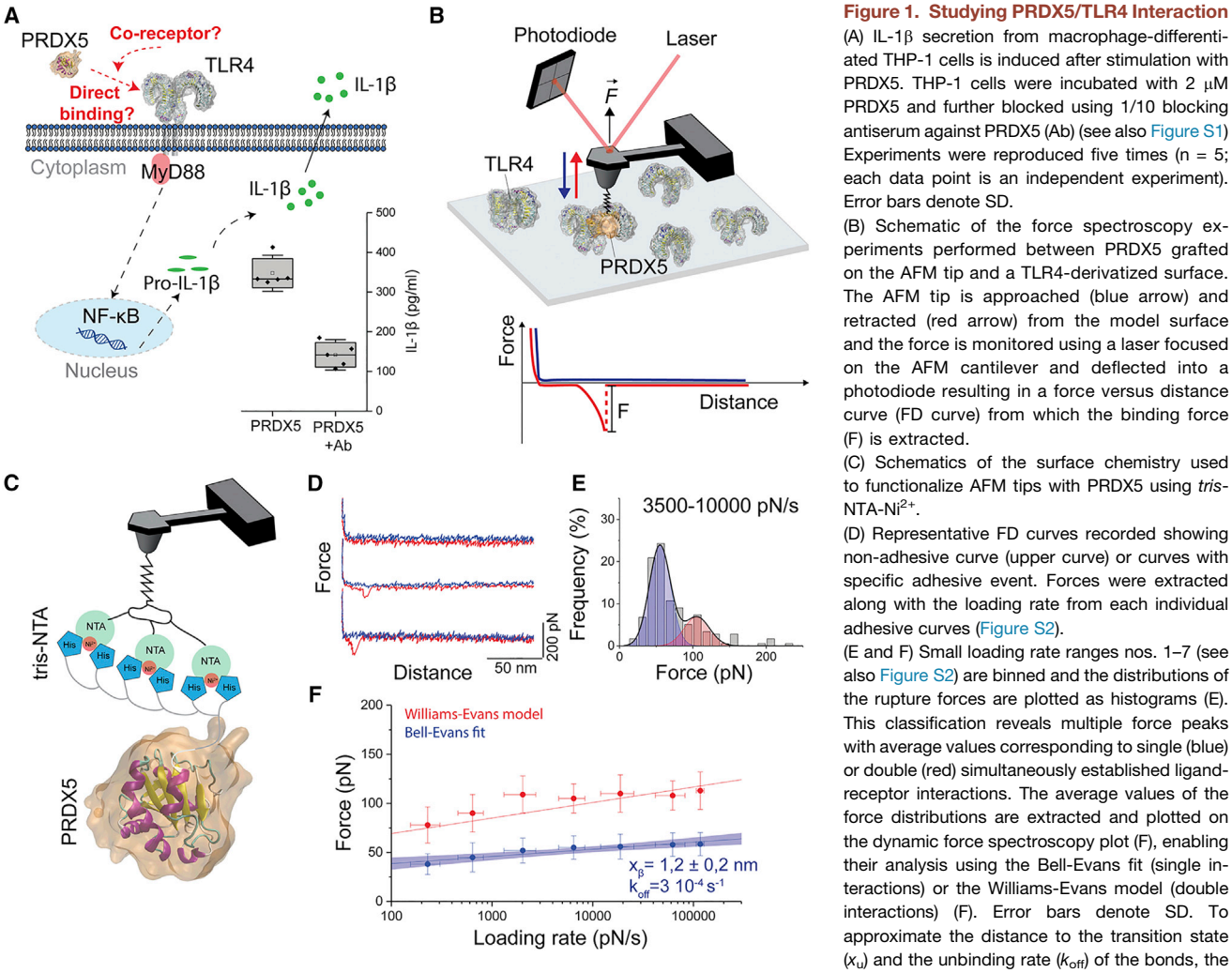

Figure 1. Studying PRDX5/TLR4 Interaction

(A) IL-1β secretion from macrophage-differentiated THP-1 cells is induced after stimulation with PRDX5. THP-1 cells were incubated with 2 μM PRDX5 and further blocked using 1/10 blocking antiserum against PRDX5 (Ab) (see also Figure S1) Experiments were reproduced five times (n = 5; each data point is an independent experiment). Error bars denote SD.

(B) Schematic of the force spectroscopy experiments performed between PRDX5 grafted on the AFM tip and a TLR4-derivatized surface. The AFM tip is approached (blue arrow) and retracted (red arrow) from the model surface and the force is monitored using a laser focused on the AFM cantilever and deflected into a photodiode resulting in a force versus distance curve (FD curve) from which the binding force (F) is extracted.

(C) Schematics of the surface chemistry used to functionalize AFM tips with PRDX5 using *tris*-NTA-Ni^{2+}.

(D) Representative FD curves recorded showing non-adhesive curve (upper curve) or curves with specific adhesive event. Forces were extracted along with the loading rate from each individual adhesive curves (Figure S2).

(E and F) Small loading rate ranges nos. 1–7 (see also Figure S2) are binned and the distributions of the rupture forces are plotted as histograms (E). This classification reveals multiple force peaks with average values corresponding to single (blue) or double (red) simultaneously established ligand-receptor interactions. The average values of the force distributions are extracted and plotted on the dynamic force spectroscopy plot (F), enabling their analysis using the Bell-Evans fit (single interactions) or the Williams-Evans model (double interactions) (F). Error bars denote SD. To approximate the distance to the transition state (x_u) and the unbinding rate (k_{off}) of the bonds, the data describing the rupture of single and multiple simultaneously occurring bonds are fitted (solid lines) by the Bell-Evans model within 95% confidence intervals (colored shaded regions). Experiments were reproduced four times independently and data were merged to extract the dynamic force spectroscopy plot.

correlates to the interaction force between cantilever tip and cell surface, and can be displayed as force-time and FD curves. Analysis of the FD curves allows the extraction of parameters including height, adhesion, contact force, sample deformation, energy dissipation, and Young's modulus (Dufrene et al., 2013). As the parameters are determined for each point of the cell surface, parametric maps can be generated and directly correlated to the AFM image. Recently, we have introduced FD-based AFM to image human G-protein-coupled receptors in proteoliposomes at high resolution (<5 nm) (Alsteens et al., 2013; Dufrene et al., 2013; Pfreundschuh et al., 2014), and we quantified the kinetic and thermodynamic parameters that describe the binding of ligands (Alsteens et al., 2015). In a second study, we introduced a chamber to keep mammalian cells in incubator-like conditions and maintain homeostasis for days (Alsteens et al., 2017b). This setup allowed us to quantify and topographically map the binding of single EnvA-RABV(ΔG) viruses at high resolution (<50 nm) on MDCK cells. Functionalized AFM tips with single viruses enabled us to detect the binding events of their receptors, and we observed a stepwise formation of virus-cell surface receptor bonds occurring with a positive allosteric modulation. Here, we examined how PRDX5 released from cells into the extracellular milieu can function as a DAMP, and can activate a cell response through direct specific binding to TLR4 receptor on living cells. To investigate the molecular mechanisms by which PRDX5 interacts with TLR4, we used AFM as a unique and novel approach in immunology to probe and map single-molecule interactions on purified receptors and on individual living cells. This single-cell approach allowed us to provide insights into fundamental processes related to the molecular cell biology of innate immunity.

Our results show that human PRDX5 is able to specifically bind to TLR4. First, we probed specific interactions at the single-molecule level between the tip derivatized with PRDX5 and TLR4 receptors immobilized on a surface. Next, we combined FD-based AFM with optical microscopy to image the binding sites of PRDX5 on macrophage-differentiated THP-1 cells, and confirmed the specific interaction with TLR4 receptors using transfected Chinese hamster ovary (CHO) cells expressing fluorescently (YFP) labeled human TLR4. Moreover,

our experimental data were supported by TLR4-PRDX5 docking simulations.

RESULTS

PRDX5 Induces Release of IL-1β by THP-1 Cells

Firstly, THP-1 cells were used to assess the role of PRDX5 as a DAMP, and to evaluate THP-1 proinflammatory cytokine release after exposure to extracellular PRDX5. THP-1 cells in the monocyte state were first differentiated into macrophage-like cells using phorbol-12-myristate-13-acetate (PMA) at 8 nM for 48 hr. Macrophage-differentiated THP-1 cells were kept for 3 hr in culture media without PMA to increase macrophage phenotype (Park et al., 2007). Exposure of macrophage-differentiated THP-1 cells to recombinant human PRDX5 resulted in the secretion of interleukin-1β (IL-1β) significantly greater than that observed in control unexposed cells but lower than after LPS exposure (Figure S1A). Preincubation of PRDX5 with blocking antibodies directed to PRDX5 significantly decreased IL-1β level release (Figures 1A and S1A). Surprisingly, IL-1β levels even increased after preincubation with PRDX5 and polymixin B used to neutralize putative residual contamination by LPS (Figure S1A). It must be noted that similar potentiation of a PRDX by polymixin B has been already observed after exposure of macrophages to PRDX1 in presence of polymixin B (Riddell et al., 2010a).

PRDX5 Interacts Specifically with TLR4 *In Vitro* in an Acellular Model

To determine whether PRDX5 could function as a DAMP by direct interaction with the cell surface receptor TLR4, we used AFM to probe the interaction between PRDX5 and TLR4 (Figure 1B). To this end, an AFM tip was functionalized with *tris*-nitrilotriacetic acids (*tris*-NTA), which shows subnanomolar affinity toward the hexahistidine (6xHis)-tagged molecule (Lata et al., 2005). The *tris*-NTA-Ni^{2+} probe was then incubated with 6xHis-PRDX5 (Figure 1C). TLR4 was covalently attached to COOH derivatized gold substrate using *N*-hydroxysuccinimide/1-ethyl-3-(3-dimethylaminopropyl)carbodiimide hydrochloride chemistry. To evaluate PRDX5 binding with TLR4, an array of 32 by 32 FD curves was recorded over a 1 μm^2 area on the TLR4-derivatized substrate. Some FD curves detected specific adhesion events (Figure 1D) at rupture distances >5 nm, and with extension patterns that can be fitted with the worm-like chain model, a biophysical model that fits the extension of proteins under an applied force.

To further determine whether these binding events were specific, we performed independent controls using (1) a tip functionalized with the *tris*-NTA-Ni^{2+} but without PRDX5 (Figure S1B), (2) the functionalized tip after blocking with the anti-PRDX5 antibody (Figure S1C), and (3) preincubation of PRDX5 with the endotoxin inactivator polymixin B (Figure S1C). These controls showed that (1) *tris*-NTA-Ni^{2+} did not interact specifically with TLR4, (2) the antibody against PRDX5 significantly reduced the interaction frequency, and (3) interactions did not involve endotoxin. This confirmed that the PRDX5 ligand linked to the tip could undergo specific interactions with TLR4.

For each adhesive curve, the force (height of the adhesive peak), as well as the loading rate (i.e., the increase of the force over time applied on the bond), were extracted. For each unbinding event, the loading rate was determined using the slope of the adhesion event measured on the force-time curve just before the rupture. The experiments were performed at six different piezo retraction speeds (Figure S2A), and all the results were sorted into seven loading rate ranges and plotted as frequency versus force histograms (Figures 1E and S2B). The histograms revealed biGaussian distributions, with the second peak centered at the double of the first one, supporting the hypothesis that the first peak is a single interaction while the second peak corresponds to double interactions. For each peak the mean and the SD were extracted and displayed in a dynamic force spectroscopy plot. The dynamic force spectroscopy plot showed that single PRDX5-TLR4 bond ruptured at forces ranging from 30 to 60 pN for loading rates between 200 and 200,000 pN s^{-1} (Figure 1F). The unbinding forces of single and multiple receptor bonds were directly proportional to the logarithmic loading rates. According to the Bell-Evans model (Evans and Ritchie, 1997; Merkel et al., 1999), such a linear increase of the unbinding force is expected when crossing a single free-energy barrier during mechanical pulling of a single ligand-receptor bond to the unbound state (Figure 1F). Using the Bell-Evans model, we extracted the separation of bond to the transition state toward the unbound state x_u = 1.2 ± 0.2 nm and the kinetic off-rate $k_{off} = 3 \times 10^{-4}\ s^{-1}$ for the single PRDX5-TLR4 bond. Remarkably, the analysis of the multiple bond rupture using the Williams-Evans model (Evans and Williams, 2002) for multiple uncorrelated bonds loaded in parallel nicely described our experimental observations (Figure 2F). This behavior has already been observed for multiple antibody-antigen interactions (Sulchek et al., 2006) or virus-receptor bonds (Alsteens et al., 2017b; Rankl et al., 2008; Sieben et al., 2012).

Imaging and Detecting PRDX5 Binding Events on Macrophage-Differentiated THP-1 Cells

Using AFM tips functionalized with PRDX5, we imaged macrophage-differentiated THP-1 cells expressing TLR4 under cell culture conditions (Figure 2A). Guided by wide-field microscopy (Figure 2B), we chose an area were multiple cells were in close proximity, which facilitated FD-based AFM topographical imaging since height differences are limited. In such an area, we recorded a height image (Figure 2B, inset), reconstructed from FD curves recorded for each topographic pixel (Figure 2C). Simultaneously, FD curves could also be analyzed and the specific adhesion events from the retraction curves were used to reconstruct the adhesion map (Figures 2D and S3A). Invisible to the naked eye, adhesive pixels were enlarged by a factor of 2, by contouring each gray pixel with two brown pixels in each direction. The specific adhesion events, with adhesion forces ranging from 80 to 500 pN, occurred at distances >50 nm separating the tip from the cell surface. The distribution of the binding events on the cell surface was homogenously distributed.

We also looked at the stiffness and, surprisingly, we observed that the cells became stiffer after 15–30 min while probed with the PRDX5-derivatized tip (Figure 2E). Stiffness was extracted using the slope of the retraction curves during cell surface indentation (see also Table S1). This observation suggests that the specific interactions between PRDX5 and THP-1 cell surface receptors induce a mechano-response. As control experiments,

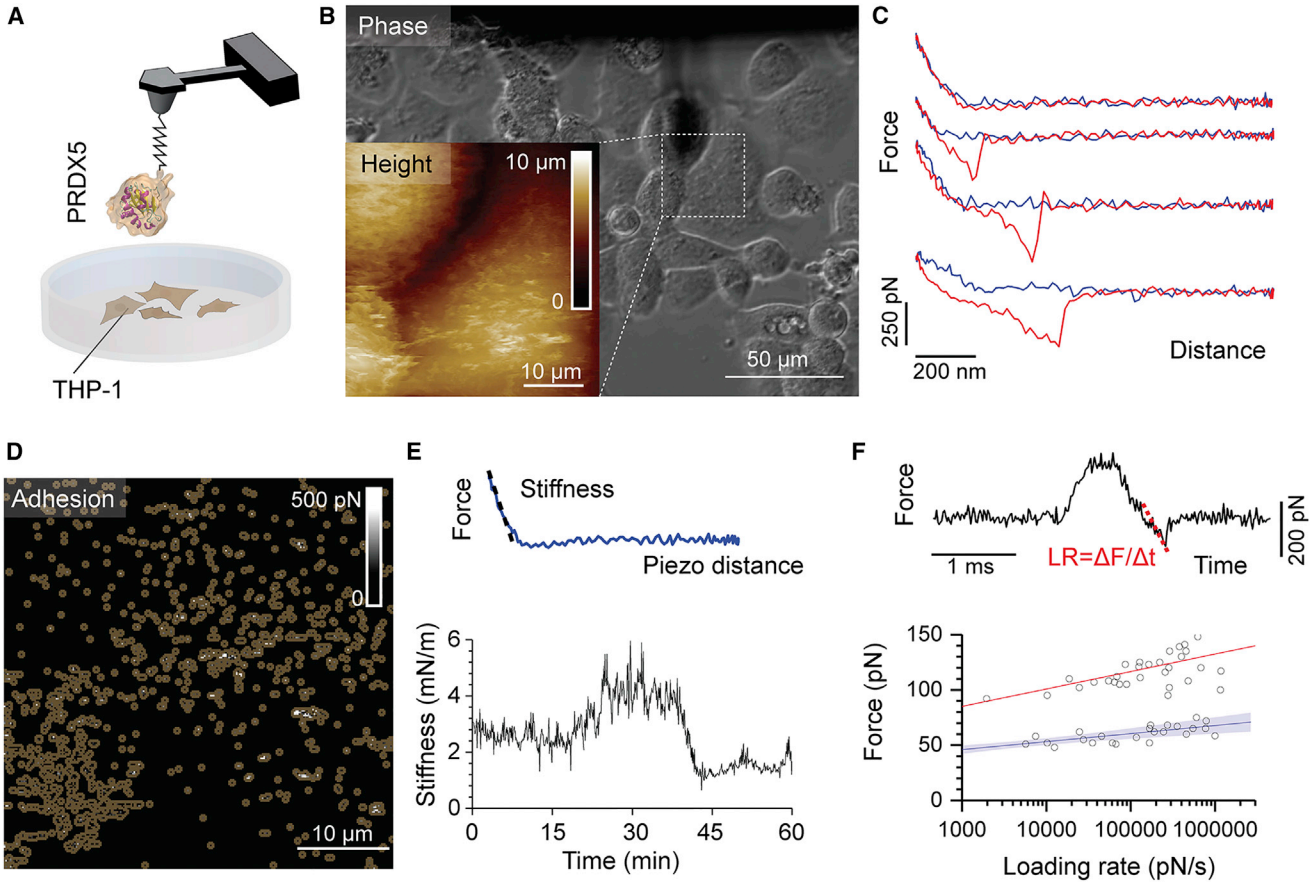

Figure 2. Mapping PRDX5 Binding to Macrophage-Differentiated THP-1 Cells Using Correlative Wide-Field Microscopy and FD-Based AFM

(A) Schematic of the FD-based AFM using an AFM tip bearing a PRDX5 molecule and living THP-1 cells. AFM experiments were performed in cell culture conditions (37°C, RPMI-1640 medium, and humidified atmosphere supplemented with 5% CO_2, see STAR Methods).

(B) Phase image showing THP-1 cells and the AFM tip placed above (see shadow). The height image recorded in the dashed square is shown in inset. AFM images were acquired using an oscillation frequency of 0.25 kHz and an amplitude of 500 nm.

(C) Representative FD curves extracted from FD-based AFM images.

(D) Corresponding adhesion channel simultaneously obtained with the height image, inset in (B). Vertical scales are given in upper right corners. Gray pixels were enlarged by a factor 2 (brown contour).

(E) Force versus piezo-distance curve showing the linear fit in the contact area used to extract the stiffness. Plot showing the evolution of the stiffness over time. Stiffness is extracted from the slope of the approach curve in the contact area.

(F) Extraction of the rupture forces separating the PRDX5 from the cell surface as well as the loading rate $LR = \Delta F/\Delta t$. For each rupture force (hollow circle, in the dynamic force spectroscopy plot below) the loading rate is extracted from the force-time curve as shown in the curve. Rupture forces (hollow circles) determined were plotted together with the fits obtained on the model surface (Figure 1F). Experiments were reproduced at least five times and other examples are shown in Figure S3.

we first probed THP-1 cells with a bare tip revealing a constant stiffness within 2 hr of AFM probing (Figure S3B). Next we probed the stiffness with a bare tip while injecting free PRDX5 at 10 and 15 μM (Figure S3B). We observed a concentration-dependent mechano-response strongly suggesting a direct relationship between PRDX5 and cell stiffening. Altogether these observations are in good agreement with a recent study performed by Preira et al. (2015) in which stiffening of THP-1 cells was observed in presence of cytokine IL-1β.

Further analysis of the adhesion force was performed to evaluate whether they are similar to the forces observed on purified TLR4. We selected FD curves with adhesion forces <150 pN, corresponding to single and double interactions *in vitro*. For each adhesive peak of these curves we extracted the adhesion force together with the loading rate (obtained from the slope before rupture, see Figure 2F). We then superimposed these values (see circles in Figure 2F) on the dynamic force spectroscopy plot obtained on the purified systems (blue and red curves for, respectively, single and double interactions, see Figure 1F), and we observed that these points very well aligned with the fits. This observation suggests that the interactions measured on living THP-1 cells are most likely similar to the PRDX5-TLR4 model system.

TLR4 Is a Specific Receptor for PRDX5 *In Vitro* in a Cellular Model

Next, we wanted to test whether TLR4 serves as a specific receptor of PRDX5 in the cellular context. CHO cells were

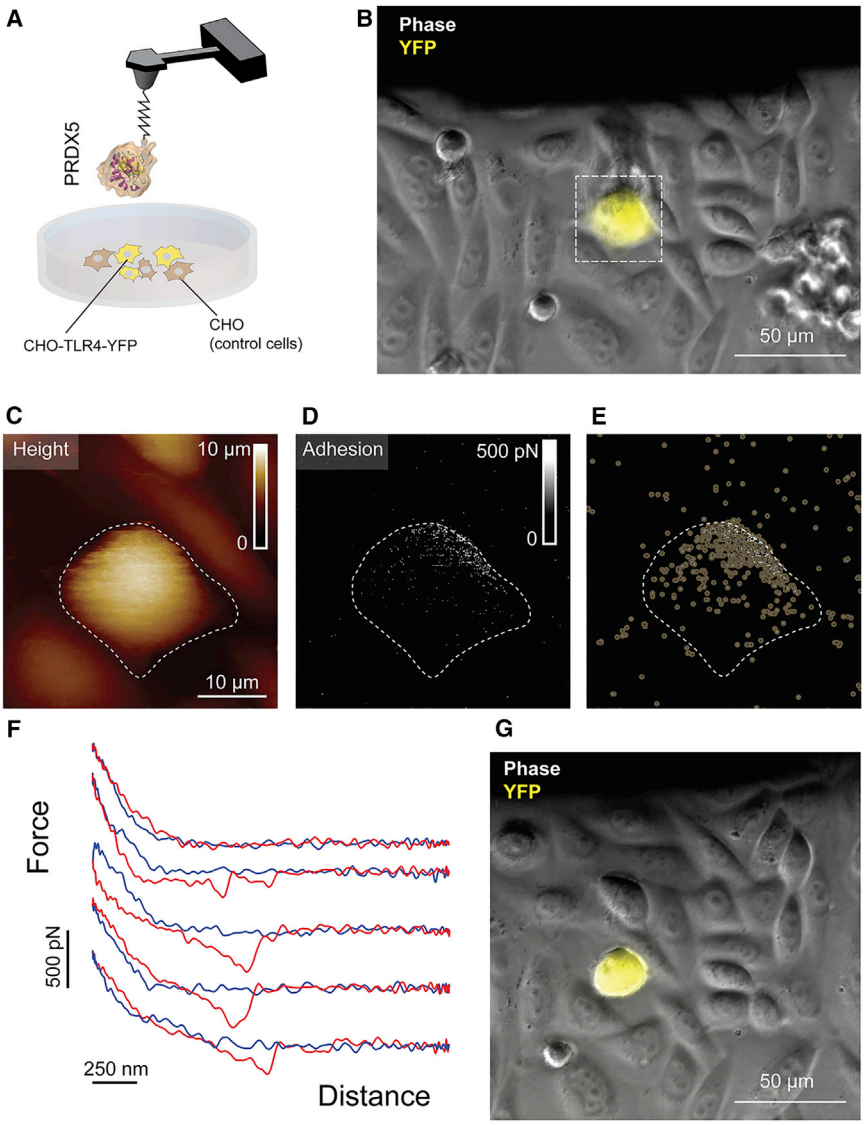

Figure 3. Mapping PRDX5 Binding to CHO-TLR4-YFP Cells Using Correlative Fluorescence Microscopy and FD-Based AFM

(A) Wild-type CHO cells were grown for 3 days before transfection with TLR4-YFP plasmid producing CHO-TLR4-YFP cells expressing TLR4-YFP (yellow).

(B) Superimposition of phase image and YFP channel showing a confluent layer of CHO cells with sparsely distributed CHO-TLR4-YFP cells.

(C) AFM height image recorded in the dashed square shown in (B).

(D and E) Adhesion image with adhesive pixels enlarged in (E). Vertical color scales are given in the upper right corner.

(F) Representative FD curves recorded from CHO-TLR4-YFP cell.

(G) Superimposition of phase image and YFP channel recorded at the end of the FD-based AFM imaging. Experiments were reproduced ten times.

transiently transfected with a construct coding for human TLR4, in fusion with the YFP, addressed to the plasma membrane, and functionally preserved (Latz et al., 2002). Using the wide-field and fluorescence signal, we chose areas in which both cell types (transfected and not transfected) were in close proximity to one another (Figures 3A and 3B). Having both CHO and CHO-TLR4-YFP cell types in a single AFM image area (40 × 40 µm) served as a direct control to evaluate whether interactions measured by the PRDX5-functionalized AFM tip were indeed due to specific binding to TLR4 receptors, and directly evaluate the extent of unspecific interactions and/or interactions with other cell surface receptors. The AFM was centered on the fluorescent cell and then the area was imaged using FD-based AFM. The topographic image (Figure 3C) and corresponding adhesion map (Figure 3D) were reconstructed from the individuals FD curves recorded. To help the visualization of the adhesion events, pixels were enlarged as mentioned above (Figure 3E). Retraction curves showed specific adhesion events mainly on CHO cells expressing the TLR4-YFP receptors (adhesive pixels are observed with a frequency >5%, n > 10,000), with adhesion forces ranging from 100 to 600 pN (Figure 3F). These specific adhesion events occurred at distances of >50 nm, corresponding to the extension of the PEG_{27} spacer, the size of the PRDX5 molecule grafted on the tip, the size of the cell surface receptor, and the cellular plasticity. FD curves recorded on non-fluorescent cells less frequently showed adhesion events (<0.25%, n > 40,000; Figure 3E).

As a control, we investigated a well-known ligand of TLR4 to ensure that the TLR receptors are well expressed at the surface of transfected CHO cells and properly folded. To this end, we functionalized the AFM tip with the high-mobility group box 1 nuclear protein (HMGB1; recombinant human 6xHis-HMGB1, Sigma) and similarly mapped the CHO-TLR4-YFP cells. Overall, adhesion events were localized on CHO-TLR4-YFP cells, while control CHO cells showed only rare events (Figure S4).

We concluded from the above experiments that the specific adhesion events measured on CHO-TLR4-YFP cells correspond to specific binding events of the PRDX5 ligand tethered to the AFM tip and the TLR4 receptors expressed at the cell surface. Surprisingly, we also observed that CHO-TLR4-YFP cells became round during AFM probing, while non-transfected cells remain spread, suggesting that the specific interaction between PRDX5 and TLR4 is causing this phenomenon (Figure 3G).

TLR4 Binding Induces Cellular Stiffening

To evaluate the change of cellular morphology during FD-based AFM using a PRDX5-derivatized tip, we scanned a small area of the cell surface in the nuclear region (100 × 100 nm, see red star in Figure 4A) for more than 1 hr and simultaneously looked at the cell morphology using optical microscopy. The size area was

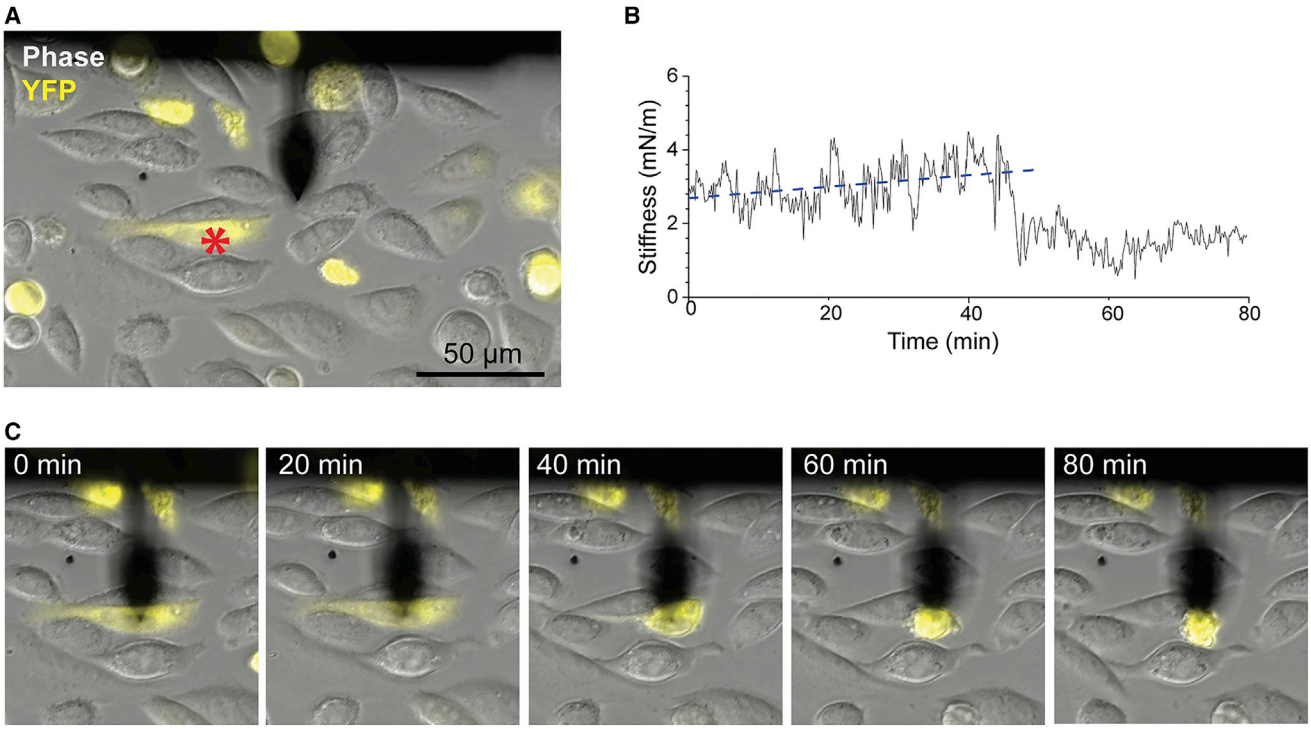

Figure 4. Probing Cellular Stiffness Evolution upon PRDX5-TLR4 Interactions on CHO-TLR4-YFP Cells

(A) Superimposition of Phase image and YFP channel showing a subconfluent layer of CHO cells with sparsely distributed CHO-TLR4-YFP cells. FD-curves were recorded on a 100 × 100 nm^2 area shown by the red asterisk.

(B and C) Plot showing the evolution of the stiffness over time. Stiffness is extracted from the slope of the approach curve in the contact area. (C) Time-lapse evolution of the cellular morphology during FD-based AFM imaging showing that the cell rounds up (see also Movie S1).

intentionally maintained small to always probe the same area (the nuclear region), so that the cellular heterogeneous stiffness has only a small influence. As shown in Figure 4, the stiffness of the cell was extracted using the slope of the extended curve in the contact region and measured over time. We observed that the cell progressively became stiffer during the first 50 min (Figures 4B and 4C). Simultaneously the cell changed its morphology from a spread state to a more round state (Figure 4C). The cell phenotype of CHO-TLR4-YFP was very similar to that observed on THP-1 cells (Figure 3G), as well as the extracted stiffness values (Table S1). In the context of endothelial inflammation, this observation is in good agreement with a recent study showing that DAMP ligands are released by pulmonary artery endothelial cells (PAECs) under stress and activate downstream PAEC inflammation through TLR2/NF-κB, resulting in the stiffening of pulmonary artery (Tan et al., 2014).

Molecular Docking Study of TLR4-PRDX5 Interaction

AFM results obtained here highly support a direct interaction between PRDX5 and TLR4. To further gain insights into PRDX5-TLR4 binding, we used molecular docking simulations. The docking was performed using ClusPro webserver (Kozakov et al., 2017) using the structure of TLR4 obtained in association with the myeloid differentiation factor 2 (MD-2) bound to LPS (PDB: 3FXI) and the oxidized form of the PDRX5 (PDB: 2VL3), which is the expected form in the oxidizing extracellular milieu (Evrard et al., 2004). Both TLR4 chains were used as center of mass and remain fixed at the origin of the coordinate, and possible rotational and translational positions of the ligand PDRX5 were evaluated at the position sampled on a sphere-based grid centered on the receptor center of mass. A Piper docking algorithm allowed evaluating the interaction energy between the two proteins taking into account van der Waals, electrostatic, and hydrophobic contributions. Docking experiment results suggest that PDRX5 predominantly interacts in the center of TLR4 crook similarly to MD-2 (Figures 5 and S5). However, due to its smaller size in comparison with MD-2, PRDX5 would only bind to a single TLR4 monomer. It must be noted that this is also experimentally supported by the AFM experiments on model surfaces where TRL4 was grafted as monomer.

DISCUSSION

Using *in vitro* acellular and cellular models, we unraveled by AFM the mechanisms by which human PRDX5 can act as a DAMP, binding to TLR4 and activating TLR4 to induce proinflammatory cytokine IL-1β release. To our knowledge, it is the first time that AFM has been used to measure DAMP interactions on the surface of living cells. Although most PRDXs have been described mainly as intracellular thiol-dependent peroxidases or protein chaperones, the role of PRDXs as PAMPs or DAMPs after their release into the extracellular milieu is now well documented in the literature. Indeed, PRDXs secreted by parasitic helminths or released by malarial *Plasmodium berghei* have been shown

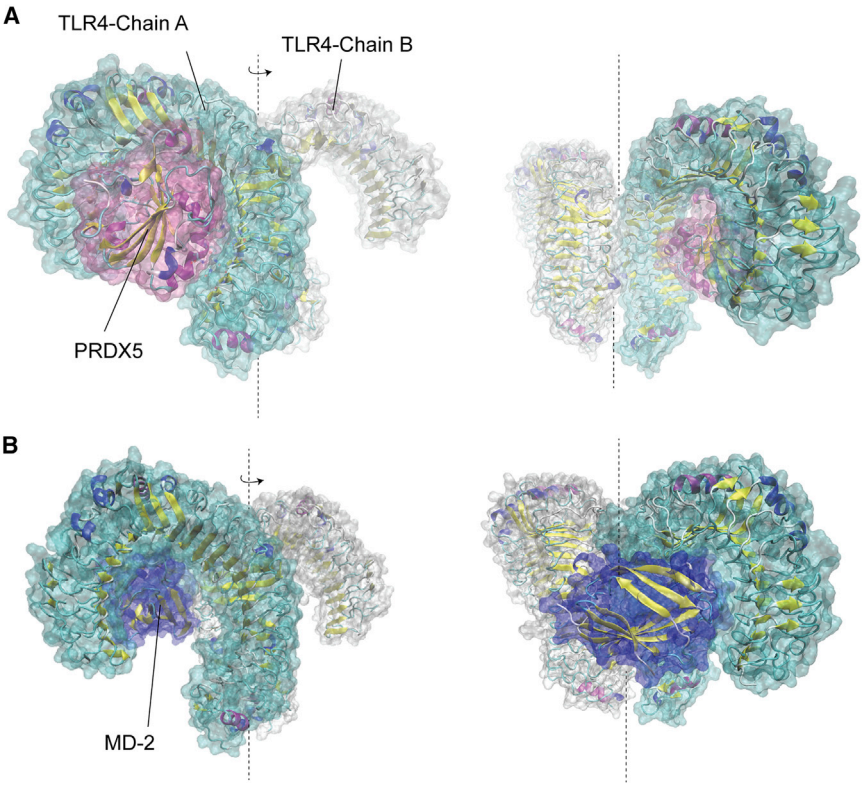

Figure 5. Docking of PRDX5 to TLR4 Structure

(A) Front view (left) and side view (right) of PRDX5 (pink colored) binding to a single chain of TLR4 (cyan-colored).

(B) Comparison with MD-2 associated to an LPS molecule bound to TLR4. For PRDX5 the simulated interaction occurs within a single TLR chain without contact to the second TLR4 chain forming the dimer. For other plausible docking positions please see Figure S5.

to act as PAMPs by, respectively, triggering the recruitment of macrophages and a Th2 response in mice, or inducing a proinflammatory response by binding to TLR4 receptors (Donnelly et al., 2005, 2008; Furuta et al., 2008). Also, before its complete characterization as a peroxidase, PRDX1 was initially described as a soluble protein released from lysed cells and exhibiting immune modulating functions able to enhance the cytotoxic activity of natural killer cells (Shau et al., 1993). More recently, mammalian PRDX1, PRDX2, PRDX4, PRDX5, and PRDX6 have been proposed to act as DAMPs through activation of TLR2 and TLR4 (Liu et al., 2016; Mullen et al., 2015; Riddell et al., 2010b; Salzano et al., 2014; Shichita et al., 2012; Zhao et al., 2016). Although mammalian PRDX5 was mainly studied so far for its role as an intracellular cytoprotective antioxidant enzyme or a redox modulator, according to its large subcellular distribution (Knoops et al., 2011), PRDX5 was also shown to play a major role as DAMP when released extracellularly from necrotic brain cells to initiate post-ischemic inflammation through activation of macrophages via TLR2 and TLR4 (Shichita et al., 2012). Therefore, in a first step, we used purified PRDX5 and TLR4 to mechanistically examine whether these receptor-ligand pairs could interact through specific binding. Using PRDX5-derivatized AFM tips and TLR4-functionalized surfaces, we observed that specific bonds are established with a rupture force ranging from 30 to 60 pN, a typical force measured for other single receptor-ligand interactions, such as RGD peptide with integrin (Lehenkari and Horton, 1999). Extraction of kinetic parameters using the Bell-Evans model revealed a highly stable interaction (very low off-rate) with an average bond lifetime of ~38 min, therefore leading to a more stable interaction than TLR4-LPS interaction (Shin et al., 2007), which has a bond lifetime of ~15 s, while TLR4 presents an intermediate bond lifetime with myeloid differentiation protein 2 (~5 min) (Han et al., 2012). Binding specificity was assessed by control experiments including blocking antibodies or endotoxin inactivator polymixin B.

Using FD-based AFM directly on living cells allowed us to demonstrate that such specific binding events similarly occur in the cellular context. Using macrophage-differentiated THP-1 cells, as a model for mimicking the function of macrophages, we probed PRDX5 binding to cell surface receptors. We furthermore observed specific interactions that shared kinetic characteristics with the model TLR4-PRDX5 system. A TLR4 role in PRDX5 binding in the cellular context was further demonstrated using CHO-TLR4-YFP cells mixed with control cells. Whether the redox status of PRDX5 may affect PRDX5-TLR4 binding would necessitate more in-depth investigation although under our experimental conditions the oxidized form of PRDX5 is expected to be the major form (Evrard et al., 2004).

FD-based AFM interactions observed between PRDX5 and TLR4 on purified receptors revealed that specific interactions occurred within either a monomeric TLR or within a single chain of a TLR4 dimer (Figure 1). Experiments on living cells provided evidence that the binding site properties are very similar to *in vitro* data, suggesting that the interaction within a single TLR4 chain site is also established on living cells. These experimental findings were further reinforced by *in silico* simulations (Figure 5). Together these data suggest that the TLR4 activation by PRDX5 is most likely very different from the TLR4 activation by LPS binding that induces receptor dimerization by contact point with the two TLR4 chains.

Surprisingly, PDRX5 binding to living cells resulted in a rapid cellular phenotype. Cells probed with a single PRDX5 molecule, even on small areas (<0.01 μm^2), became stiffer. To the best of our knowledge this is the first direct evidence that DAMPs binding through TLR4 induces a mechano-response by the cells, and is particularly relevant in the context of inflammation. Increasing evidence shows that, for example, artery stiffening or reduced arterial compliance is a prominent feature of systemic hypertension, pulmonary hypertension, and other vascular-related diseases (Preira et al., 2015). However, so far, the mechanism

underlying such stiffening remains elusive. Our study illustrates a new potential mechanism for how cellular mechanical stiffening is triggered downstream of the inflammation site by direct specific binding to TLR4.

In the future, the combined fluorescence-nanoscopic approach used in this work could help to characterize more deeply the role of different ligands binding to immune receptors in living cells. Moreover, our quantitative method could not only help to uncover the receptors involved in the triggering of the immune response, but could also provide a tool to quantify the effects of molecules interfering with receptor activation and therefore aid the development of novel drugs modulating the inflammatory response.

SIGNIFICANCE

Inflammation is induced when innate immune cells, such as macrophages, detect danger molecules during infection or tissue injury. Among such molecules, PRDXs were shown recently to act as factors released by damaged or dying cells, termed DAMPs. However, the molecular mechanisms of how extracellular PRDXs act as DAMPs, interact with pattern-recognition receptors, and contribute to the induction of inflammation by modulating proinflammatory cytokine release are still unclear. Moreover, a better understanding of these mechanisms could help developing new therapeutic approaches for inflammation-related diseases. Here, we examined at the nanoscopic scale the interactions between PRDX5, previously shown to act as a DAMP, and TLR4, using AFM in acellular and cellular models. We demonstrated that PRDX5 specifically binds to TLR4. Surprisingly, this binding triggers also a cellular mechanoresponse, suggesting that PRDX5-TLR4 interactions not only modulate proinflammatory cytokine release but also cell stiffening, which could be highly relevant in the inflammatory response. Indeed, increasing evidence shows that, for example, artery stiffening or reduced arterial compliance is a prominent feature of systemic hypertension, pulmonary hypertension, and other vascular diseases with an inflammatory component. However, so far, the mechanism underlying such coupling remained elusive. Our study illustrates a new potential mechanism of how cellular mechanical stiffening is triggered during inflammation by a direct specific binding to TLR4. Our study demonstrates also the potential of AFM as a multifunctional approach to simultaneously characterize both ligand binding and mechanical properties.

STAR★METHODS

Detailed methods are provided in the online version of this paper and include the following:

- KEY RESOURCES TABLE
- CONTACT FOR REAGENT AND RESOURCE SHARING
- EXPERIMENTAL MODEL AND SUBJECT DETAILS
- METHODS DETAILS
  - TLR4-YFP Expressing CHO Cells (CHO-TLR4-YFP)
  - Production and Purification of Recombinant Human PRDX5
  - Differentiation of THP-1 Cells into Macrophages
  - Quantification of Human IL-1β
  - Functionalization of AFM Tips
  - Single-Molecule Force Spectroscopy on Model Surfaces
  - Combined FD-Based AFM and Optical Microscopy
  - Analysis of Force Curves
  - Extraction of Kinetic Parameters
  - Molecular Docking
- QUANTIFICATION AND STATISTICAL ANALYSIS
- DATA AND SOFTWARE AVAILABILITY

SUPPLEMENTAL INFORMATION

Supplemental Information includes five figures, one table, and one movie and can be found with this article online at https://doi.org/10.1016/j.chembiol.2018.02.006.

ACKNOWLEDGMENTS

The research of the authors is financially supported by the Fonds National de la Recherche Scientifique (F.R.S.-FNRS grant numbers: PDR T.0090.15 to B.K. and PDR T.0070.16 to D.A.) and the Fédération Wallonie-Bruxelles. D.A. is a Research Associate of the FRS-FNRS.

AUTHOR CONTRIBUTIONS

D.A. and B.K. designed the experiments. A.C. produced PRDX5 and performed IL-1β assays. A.C., J.G., and S.B. transfected CHO cells. S.B. provided differentiated THP-1 cells. D.A., S.D., and M.A.P. performed AFM experiments. D.A., S.D., and M.A.P. co-analyzed the experimental and calculated data. All authors wrote the paper.

DECLARATION OF INTERESTS

The authors declare no competing interests.

Received: October 24, 2017
Revised: January 8, 2018
Accepted: February 7, 2018
Published: March 15, 2018

REFERENCES

Alsteens, D., Trabelsi, H., Soumillion, P., and Dufrene, Y.F. (2013). Multiparametric atomic force microscopy imaging of single bacteriophages extruding from living bacteria. Nat. Commun. *4*, 2926.

Alsteens, D., Pfreundschuh, M., Zhang, C., Spoerri, P.M., Coughlin, S.R., Kobilka, B.K., and Muller, D.J. (2015). Imaging G protein-coupled receptors while quantifying their ligand-binding free-energy landscape. Nat. Methods *12*, 845–851.

Alsteens, D., Gaub, H.E., Newton, R., Pfreundschuh, M., Gerber, C., and Müller, D.J. (2017a). Atomic force microscopy-based characterization and design of biointerfaces. Nat. Rev. Material *2*, 17008.

Alsteens, D., Newton, R., Schubert, R., Martinez-Martin, D., Delguste, M., Roska, B., and Müller, D.J. (2017b). Nanomechanical mapping of first binding steps of a virus to animal cells. Nat. Nanotechnol. *12*, 177–183.

Binnig, G., Quate, C.F., and Gerber, C. (1986). Atomic force microscope. Phys. Rev. Lett. *56*, 930–933.

Butt, H.J., and Jaschke, M. (1995). Calculation of thermal noise in atomic-force microscopy. Nanotechnol *6*, 1–7.

Chen, G.Y., and Nunez, G. (2010). Sterile inflammation: sensing and reacting to damage. Nat. Rev. Immunol. *10*, 826–837.

Chou, J.L., Wu, C.H., Tsai, C.Y., Chang, A.Y., and Chan, S.H. (2011). Proteomic investigation of a neural substrate intimately related to brain death. Proteomics *11*, 239–248.

Dayon, L., Turck, N., García-Berrocoso, T., Walter, N., Burkhard, P.R., Vilalta, A., Sahuquillo, J., Montaner, J., and Sanchez, J.-C. (2011). Brain extracellular fluid protein changes in acute stroke patients. J. Proteome Res. *10*, 1043–1051.

Declercq, J.P., Evrard, C., Clippe, A., Stricht, D.V., Bernard, A., and Knoops, B. (2001). Crystal structure of human peroxiredoxin 5, a novel type of mammalian peroxiredoxin at 1.5 Å resolution. J. Mol. Biol. *311*, 751–759.

Donnelly, S., O'Neill, S.M., Sekiya, M., Mulcahy, G., and Dalton, J.P. (2005). Thioredoxin peroxidase secreted by *Fasciola hepatica* induces the alternative activation of macrophages. Infect. Immun. *73*, 166–173.

Donnelly, S., Stack, C.M., O'Neill, S.M., Sayed, A.A., Williams, D.L., and Dalton, J.P. (2008). Helminth 2-Cys peroxiredoxin drives Th2 responses through a mechanism involving alternatively activated macrophages. FASEB J. *22*, 4022–4032.

Dufrene, Y.F., Martinez-Martin, D., Medalsy, I., Alsteens, D., and Muller, D.J. (2013). Multiparametric imaging of biological systems by force-distance curve-based AFM. Nat. Methods *10*, 847–854.

Dufrene, Y.F., Ando, T., Garcia, R., Alsteens, D., Martinez-Martin, D., Engel, A., Gerber, C., and Muller, D.J. (2017). Imaging modes of atomic force microscopy for application in molecular and cell biology. Nat. Nanotechnol. *12*, 295–307.

Evans, E., and Ritchie, K. (1997). Dynamic strength of molecular adhesion bonds. Biophys. J. *72*, 1541–1555.

Evans, E., and Williams, P. (2002). Dynamic force spectroscopy. In Physics of Bio-molecules and Cells, H. Flyvbjerg, f. Jülicher, P. Orms, and F. David, eds. (Pringer), pp. 145–204.

Evrard, C., Capron, A., Marchand, C., Clippe, A., Wattiez, R., Soumillion, P., Knoops, B., and Declercq, J.P. (2004). Crystal structure of a dimeric oxidized form of human peroxiredoxin 5. J. Mol. Biol. *337*, 1079–1090.

Furuta, T., Imajo-Ohmi, S., Fukuda, H., Kano, S., Miyake, K., and Watanabe, N. (2008). Mast cell-mediated immune responses through IgE antibody and Toll-like receptor 4 by malarial peroxiredoxin. Eur. J. Immunol. *38*, 1341–1350.

Goemaere, J., and Knoops, B. (2012). Peroxiredoxin distribution in the mouse brain with emphasis on neuronal populations affected in neurodegenerative disorders. J. Comp. Neurol. *520*, 258–280.

Han, J., Kim, H.J., Lee, S.-C., Hong, S., Park, K., Jeon, Y.H., Kim, D., Cheong, H.-K., and Kim, H.-S. (2012). Structure-based rational design of a toll-like receptor 4 (TLR4) decoy receptor with high binding affinity for a target protein. PLoS One *7*, e30929.

Ishii, T., Warabi, E., and Yanagawa, T. (2012). Novel roles of peroxiredoxins in inflammation, cancer and innate immunity. J. Clin. Biochem. Nutr. *50*, 91–105.

Knoops, B., Goemaere, J., Van der Eecken, V., and Declercq, J.P. (2011). Peroxiredoxin 5: structure, mechanism, and function of the mammalian atypical 2-Cys peroxiredoxin. Antioxid. Redox Signal. *15*, 817–829.

Knoops, B., Argyropoulou, V., Becker, S., Ferté, L., and Kuznetsova, O. (2016). Multiple roles of peroxiredoxins in inflammation. Mol. Cells *39*, 60–64.

Kono, H., and Rock, K.L. (2008). How dying cells alert the immune system to danger. Nat. Rev. Immunol. *8*, 279–289.

Kozakov, D., Hall, D.R., Xia, B., Porter, K.A., Padhorny, D., Yueh, C., Beglov, D., and Vajda, S. (2017). The ClusPro web server for protein-protein docking. Nat. Protoc. *12*, 255–278.

Kumar, S., Ingle, H., Prasad, D.V., and Kumar, H. (2013). Recognition of bacterial infection by innate immune sensors. Crit. Rev. Microbiol. *39*, 229–246.

Lata, S., Reichel, A., Brock, R., Tampé, R., and Piehler, J. (2005). High-affinity adaptors for switchable recognition of histidine-tagged proteins. J. Am. Chem. Soc. *127*, 10205–10215.

Latz, E., Visintin, A., Lien, E., Fitzgerald, K.A., Monks, B.G., Kurt-Jones, E.A., Golenbock, D.T., and Espevik, T. (2002). Lipopolysaccharide rapidly traffics to and from the Golgi apparatus with the toll-like receptor 4-MD-2-CD14 complex in a process that is distinct from the initiation of signal transduction. J. Biol. Chem. *277*, 47834–47843.

Lehenkari, P.P., and Horton, M.A. (1999). Single integrin molecule adhesion forces in intact cells measured by atomic force microscopy. Biochem. Biophys. Res. Commun. *259*, 645–650.

Liu, D.L., Zhao, L.X., Zhang, S., and Du, J.R. (2016). Peroxiredoxin 1-mediated activation of TLR4/NF-kappaB pathway contributes to neuroinflammatory injury in intracerebral hemorrhage. Int. Immunopharmacol. *41*, 82–89.

Merkel, R., Nassoy, P., Leung, A., Ritchie, K., and Evans, E. (1999). Energy landscapes of receptor-ligand bonds explored with dynamic force spectroscopy. Nature *397*, 50–53.

Mullen, L., Hanschmann, E.M., Lillig, C.H., Herzenberg, L.A., and Ghezzi, P. (2015). Cysteine oxidation targets peroxiredoxins 1 and 2 for exosomal release through a novel mechanism of redox-dependent secretion. Mol. Med. *21*, 98–108.

Park, E.K., Jung, H.S., Yang, H.I., Yoo, M.C., Kim, C., and Kim, K.S. (2007). Optimized THP-1 differentiation is required for the detection of responses to weak stimuli. Inflamm. Res. *56*, 45–50.

Park, M.H., Jo, M., Kim, Y.R., Lee, C.K., and Hong, J.T. (2016). Roles of peroxiredoxins in cancer, neurodegenerative diseases and inflammatory diseases. Pharmacol. Ther. *163*, 1–23.

Perkins, A., Nelson, K.J., Parsonage, D., Poole, L.B., and Karplus, P.A. (2015). Peroxiredoxins: guardians against oxidative stress and modulators of peroxide signaling. Trends Biochem. Sci. *40*, 435–445.

Pfreundschuh, M., Martinez-Martin, D., Mulvihill, E., Wegmann, S., and Muller, D.J. (2014). Multiparametric high-resolution imaging of native proteins by force-distance curve-based AFM. Nat. Protoc. *9*, 1113–1130.

Preira, P., Forel, J.-M., Robert, P., Nègre, P., Biarnes-Pelicot, M., Xeridat, F., Bongrand, P., Papazian, L., and Theodoly, O. (2015). The leukocyte-stiffening property of plasma in early acute respiratory distress syndrome (ARDS) revealed by a microfluidic single-cell study: the role of cytokines and protection with antibodies. Crit. Care *20*, 8.

Rankl, C., Kienberger, F., Wildling, L., Wruss, J., Gruber, H.J., Blaas, D., and Hinterdorfer, P. (2008). Multiple receptors involved in human rhinovirus attachment to live cells. Proc. Natl. Acad. Sci. USA *105*, 17778–17783.

Rhee, S.G., and Kil, I.S. (2017). Multiple functions and regulation of mammalian peroxiredoxins. Annu. Rev. Biochem. *86*, 749–775.

Riddell, J.R., Wang, X.Y., Minderman, H., and Gollnick, S.O. (2010a). Peroxiredoxin 1 stimulates secretion of pro-inflammatory cytokines by binding to toll-like receptor 4. J. Immunol. *184*, 1022–1030.

Riddell, J.R., Wang, X.Y., Minderman, H., and Gollnick, S.O. (2010b). Peroxiredoxin 1 stimulates secretion of proinflammatory cytokines by binding to TLR4. J. Immunol. *184*, 1022–1030.

Robinson, M.W., Hutchinson, A.T., Dalton, J.P., and Donnelly, S. (2010). Peroxiredoxin: a central player in immune modulation. Parasite Immunol. *32*, 305–313.

Salzano, S., Checconi, P., Hanschmann, E.M., Lillig, C.H., Bowler, L.D., Chan, P., Vaudry, D., Mengozzi, M., Coppo, L., Sacre, S., et al. (2014). Linkage of inflammation and oxidative stress via release of glutathionylated peroxiredoxin-2, which acts as a danger signal. Proc. Natl. Acad. Sci. USA *111*, 12157–12162.

Shau, H., Gupta, R.K., and Golub, S.H. (1993). Identification of a natural killer enhancing factor (NKEF) from human erythroid cells. Cell Immunol. *147*, 1–11.

Shichita, T., Hasegawa, E., Kimura, A., Morita, R., Sakaguchi, R., Takada, I., Sekiya, T., Ooboshi, H., Kitazono, T., Yanagawa, T., et al. (2012). Peroxiredoxin family proteins are key initiators of post-ischemic inflammation in the brain. Nat. Med. *18*, 911–917.

Shin, H.J., Lee, H., Park, J.D., Hyun, H.C., Sohn, H.O., Lee, D.W., and Kim, Y.S. (2007). Kinetics of binding of LPS to recombinant CD14, TLR4, and MD-2 proteins. Mol. Cells *24*, 119–124.

Sieben, C., Kappel, C., Zhu, R., Wozniak, A., Rankl, C., Hinterdorfer, P., Grubmuller, H., and Herrmann, A. (2012). Influenza virus binds its host cell using multiple dynamic interactions. Proc. Natl. Acad. Sci. USA *109*, 13626–13631.

Sulchek, T., Friddle, R.W., and Noy, A. (2006). Strength of multiple parallel biological bonds. Biophys. J. *90*, 4686–4691.

Tan, Y., Tseng, P.-O., Wang, D., Zhang, H., Hunter, K., Hertzberg, J., Stenmark, K.R., and Tan, W. (2014). Stiffening-induced high pulsatility flow activates endothelial inflammation via a TLR2/NF-κB pathway. PLoS One *9*, e102195.

Verbelen, C., Christiaens, N., Alsteens, D., Dupres, V., Baulard, A.R., and Dufrêne, Y.F. (2009). Molecular mapping of lipoarabinomannans on mycobacteria. Langmuir *25*, 4324–4327.

Wildling, L., Unterauer, B., Zhu, R., Rupprecht, A., Haselgrübler, T., Rankl, C., Ebner, A., Vater, D., Pollheimer, P., Pohl, E.E., et al. (2011). Linking of sensor molecules with amino groups to amino-functionalized AFM tips. Bioconjug. Chem. *22*, 1239–1248.

Zhao, L.X., Du, J.R., Zhou, H.J., Liu, D.L., Gu, M.X., and Long, F.Y. (2016). Differences in proinflammatory property of six subtypes of peroxiredoxins and anti-inflammatory effect of ligustilide in macrophages. PLoS One *11*, e0164586.

Please cite this article in press as: Knoops et al., Specific Interactions Measured by AFM on Living Cells between Peroxiredoxin-5 and TLR4: Relevance for Mechanisms of Innate Immunity, Cell Chemical Biology (2018), https://doi.org/10.1016/j.chembiol.2018.02.006

STAR★METHODS

KEY RESOURCES TABLE

REAGENT or RESOURCE	SOURCE	IDENTIFIER
Chemicals, Peptides, and Recombinant Proteins		
LPS from Escherichia coli O111:B4	Sigma-Aldrich	Cat#L2630
PRDX5, N-terminal 6xHis-tagged, human	Declercq et al., 2001	N/A
6xHis-HMGB1	Sigma-Aldrich	Cat#H4652
Lipofectamine 2000	ThermoFisher	Cat#11668030
OptiMEM	Gibco	Cat#31985-062
EndoTrap HD kit	Hyglos	Cat#800053
DMEM high glucose	Life Technologies	Cat#61965-026
Fetal Bovine Serum	Lonza	Cat#DE 14-802F
Penicillin-Streptomycin	Life Technologies	Cat#15140-122
RPMI-1640 GlutaMAX	Life Technologies	Cat#61870-010
Phorbol-12-myristate-13-acetate (PMA)	Sigma-Aldrich	Cat#P8139
Antiserum directed to human PRDX5	Goemaere and Knoops, 2012	N/A
Polymixin B	Sigma-Aldrich	Cat#81271
NHS-PEG_{27}-acetal linker	Wildling et al., 2011	N/A
Citric acid	Sigma-Aldrich	Cat#251275
tris-NTA Trifluoroacetic Acid Salt	Toronto Research Chemicals	Cat#N925005
Cyanoborhydride	Sigma-Aldrich	Cat#156159
Ethanolamine hydrochloride	Sigma-Aldrich	Cat#E6133
$NiCl_2$	Sigma-Aldrich	Cat#339350
Critical Commercial Assays		
Quantikine ELISA human IL-1β	R&D Systems	Cat#DLB50
Experimental Models: Cell Lines		
THP-1	ATCC	ATCC TIB-202
CHO (CHO-K1)	ATCC	ATCC CRL-9618
Recombinant DNA		
pcDNA3-TLR4-YFP	Latz et al., 2002	Addgene Plasmid #13018
Software and Algorithms		
Nanoscope Analysis software	Bruker	N/A
Origin	OriginLab	N/A
Other		
MSCT AFM tips	Bruker	Cat#MSCT
Peak-Force QNM-Live cells AFM tips	Bruker	Cat#PF-QNM-Lc

CONTACT FOR REAGENT AND RESOURCE SHARING

Further information and requests for resources and reagents should be directed to and will be fulfilled by the Lead Contact, David Alsteens (david.alsteens@uclouvain.be).

EXPERIMENTAL MODEL AND SUBJECT DETAILS

Chinese Hamster Ovary (CHO-K1) cells (ATCC) were cultured in DMEM (Life Technologies) with 10% FBS (Lonza), with 100 μg mL^{-1} penicillin and 100 μg mL^{-1} streptomycin (Life Technologies) at 37°C in humidified atmosphere supplemented with 5% CO_2. THP-1

cells (ATCC), an acute monocytic leukemia cell line from a 1 year old male infant, were cultured in RPMI-1640-GlutaMAX (Life Technologies) supplemented with 10% FBS (Lonza), and 100 μg mL^{-1} penicillin and 100 μg mL^{-1} streptomycin (Life Technologies) at 37°C in humidified atmosphere supplemented with 5% CO_2.

METHODS DETAILS

TLR4-YFP Expressing CHO Cells (CHO-TLR4-YFP)

CHO cells (provided by Prof. Y-J Schneider, UCL, Belgium) were plated at a density of ~ 0.5 × 10^6 cells in 40 mm culture dishes with 2 mL of Dulbecco's modified eagle medium–high glucose (Sigma-Aldrich) supplemented with 10% fetal bovine serum (FBS) (DMEM/High-10), 100 μg mL^{-1} penicillin and 100 μg mL^{-1} streptomycin (Life Technologies) at 37°C in humidified atmosphere supplemented with 5% CO_2. Cells were transiently transfected with 3.25μg of pcDNA3-TLR4-YFP (Addgene, plasmid #13018, gift of Dr. D. Golenbock, University of Massachusetts Medical School, USA) using 6.5μL Lipofectamine 2000 (ThermoFisher) in 325μL of OptiMEM (Gibco). Culture medium was changed after 24h and Petri dishes were used for AFM experiments after 48-72h.

Production and Purification of Recombinant Human PRDX5

The expression and purification of recombinant N-terminal 6xHis-tagged human PRDX5 were described previously (Declercq et al., 2001). First strand cDNA was obtained with Moloney leukemia virus reverse transcriptase (Superscript II, Life Technologies) from 2 μg of human lung RNA using oligo(dT)25 as primer according to the manufacturer's instructions. Human PRDX5 cDNA was PCR amplified using forward primer 5'-GCTGCAGGATCCGCCCCAATCAAGGTGGGAG-3' (*Bam*HI site underlined) and reverse primer 5'-GGCCCAAAGCTTCAGAGCTGTGAGATGATA-3' (*Hind*III site underlined). The PCR product was digested with *Bam*HI and *Hind*III, and ligated into the pQE-30 expression vector (Qiagen). The insert was sequenced and the N-terminal fusion with the hexahistidine (6xHis) tag was confirmed. The resulting vector was used to transform *E. coli* strain M15 (pRep4). *E. coli* were grown at 37°C in LB medium containing 1 mM IPTG. Pelleted cells were lysed in 10 mM imidazole, 50 mM phosphate, 300 mM NaCl (pH 8) by sonication and clarified by centrifugation. The supernatant containing 6xHis-tagged PRDX5 was loaded onto a Ni^{2+}-NTA column (Qiagen). The column was washed and the protein was eluted with 50 mM phosphate, 300 mM NaCl, 250 mM imidazole (pH 8). Eluted protein was then dialysed against PBS (pH 7.2). Putative contaminating endotoxins were removed using EndoTrap HD kit (Hyglos) and the recombinant protein was collected in PBS at 0.9mg/mL.

Differentiation of THP-1 Cells into Macrophages

The human monocytic cell line THP-1 (provided by Prof. C. Remacle, UCL, Belgium) was cultured in RPMI-1640, GlutaMAX (Life Technologies) supplemented with 10% FBS (Lonza), 100 U/ml streptomycin and 100 U/ml penicillin (Life Technologies). THP-1 cells were maintained at 37°C in 5% CO_2. THP-1 cells were differentiated into macrophages via exposure to 8 nM PMA (Sigma-Aldrich) in 96-well plates or 40 mm culture dishes in, respectively, 100 μl or 3 mL of RPMI-1640-GlutaMAX (Life Technologies) supplemented with 10% FBS (Lonza) and 100 U/ml streptomycin and 100 U/ml penicillin (Life Technologies) for 48h according to (Park et al., 2007).

Quantification of Human IL-1β

Macrophage-differentiated THP-1 cells cultured in 96-well plates were exposed to 2 μM of purified recombinant human PRDX5 (Declercq et al., 2001), 1/10 antiserum directed to human PRDX5 (Goemaere and Knoops, 2012), 30 μg/ml polymixin B and 1 μg/ml LPS (from *Escherichia coli* O111:B4, Sigma-Aldrich) in RPMI-1640-GlutaMAX (Life Technologies) supplemented with 100 U/ml streptomycin and 100 U/ml penicillin (Life Technologies) without FBS. Culture medium was harvested 48h after cell exposure and IL-1β was measured, using Quantikine ELISA human IL-1β (R&D Systems).

Functionalization of AFM Tips

To functionalize AFM tips we used NHS-PEG_{27}-acetal linkers (Wildling et al., 2011). The cantilevers were immersed in 1 mL of citric acid (1%, w/v) for 10 min. After washing the cantilevers three times for 5 min in MilliQ water, they were dried with N_2. The cantilevers were immersed in a 100 μL droplet of the amino-*tris*-NTA molecule (αS,α'S,α''S)-11-(6-amino-1-oxohexyl)-α,α',α''-*tris*[bis(carboxymethyl)amino]-δ,δ',δ''-trioxo-1,4,8,11 tetraazacyclotetra-decane-1,4,8-tripentanoic acid, Toronto Research Chemicals, Toronto, Ontario, Canada) (2 mM in PBS). 2 μL of a 1 M cyanoborhydride solution were added and mixed carefully. The cantilevers were incubated for 2 h. The reaction was quenched by adding 5 μL of 1 M ethanolamine (pH 8.0). After 10 min, the cantilevers were washed in PBS three times for 5 min and immersed in 5 mM $NiCl_2$ for 10 min. Then, the *tris*-NTA-Ni^{2+} AFM tips were incubated for 2h in a solution of His_6-PRDX5 or 6xHis-HMGB1 at 0.2 mg/mL. Finally the cantilevers were washed in PBS three times for 5 min and transferred to a multiwell plate filled with PBS buffer. Cantilevers were used in AFM experiments the same day as the last step of the functionalization protocol.

Single-Molecule Force Spectroscopy on Model Surfaces

SMFS measurements were performed using the PRDX5 functionalized tips (see above mentioned protocol) using MSCT tips (k=0.01 N/m) (Bruker Corporation, Santa Barbara, CA) and substrates functionalized with TLR4 at room temperature (20°C) in PBS buffer using a Nanoscope VIII Multimode AFM (Bruker Corporation, Santa Barbara, CA). Recombinant TLR4 was immobilized onto gold substrates using N-hydroxysuccinimide (NHS) (Sigma-Aldrich) and 1-ethyl-3-(3-dimethylaminopropyl)-carbodiimide (EDC)

as described previously (Verbelen et al., 2009). The activated surfaces were then incubated with 100 μg/mL TLR4 (R&D Systems) in PBS. Multiple force curves were recorded at 0 ms contact time, with a maximum applied force of 250 pN, and using a constant approach speed of 1,000 nm/s and retraction speeds of 100 nm/s, 200 nm/s, 500 nm/s, 1,000 nm/s, 2,000 nm/s and 10,000 nm/s. For each experiment, these speeds were recorded in different order. Cantilevers were first calibrated on glass using thermal noise method (Butt and Jaschke, 1995), yielding values ranging from 0.011–0.023 N m^{-1}.

Combined FD-Based AFM and Optical Microscopy

Correlative microscopy was acquired on an AFM (Bioscope Catalyst, Bruker Corporation, Santa Barbara, CA) operated in the PeakForce QNM mode (Nanoscope software v9.1) to conduct FD-based AFM and coupled on an inverted epifluorescence microscope (Axio observer Z1, Zeiss). The AFM was equipped with a 150 μm piezoelectric scanner. Overview images (~40 x 40 μm^2) were recorded at imaging forces of ~350-750 pN using PeakForce QNM-Live Cell (PFQNM-LC) cantilevers (Bruker Corporation, Santa Barbara, CA) having tip lengths of 17 μm, tip radii of 65 nm and opening angles of 15°. All microscopy and FD-based AFM imaging was performed at cell culture conditions using the combined AFM and optical microscopy chamber at 37°C in medium supplemented with 10% FBS. A gas mixture of synthetic air supplemented with 5% CO_2 at 95% relative humidity using a gas humidifier membrane (PermSelect silicone) was blown at 0.1 L min^{-1} into the microscopy chamber. The humidity was controlled using a humidity sensor (Sensirion). The Cantilevers were first calibrated on glass using thermal noise method (Butt and Jaschke, 1995), yielding values ranging from 0.061–0.102 N m^{-1}. The AFM tip was oscillated vertically at 0.25 kHz applying 300–1,000 nm amplitudes in the PeakForce QNM mode. The sample was scanned using a frequency of 0.125 Hz and 256 pixels per line (256 lines). AFM images and force curves were analyzed using the Nanoscope analysis software (v1.8, Bruker).

Analysis of Force Curves

Individual force curves detecting unbinding events of the protein were analysed using the Nanoscope analysis software. The base line of the retraction curve was corrected using a linear fit on the last 30% of the retraction curve. Using the force-time curve the loading rate (slope) of each rupture event was approached by dividing the force segment ΔF through the time segment Δt (Figure 2F).

Extraction of Kinetic Parameters

Origin software (OriginLab) was used to fit the loading rate-dependent interaction forces using a linear iterative fitting algorithm (Levenberg Marquardt) along with the Bell-Evans model (Evans and Williams, 2002). Each iteration computed a chi-square value (χ^2) after which the parameter values were adjusted to reduce χ^2. When the difference between two consecutive χ^2 values computed in two successive iterations was small enough (tolerance 10^{-15}), the fitting procedure converged. We fixed the maximum number of iterations to 200. To evaluate the validity of the fit, we also checked if the adjusted R^2 (coefficient of determination) was >0.75 and looked at the residual plot and the Q-Q plot.

Molecular Docking

The oxidized form of PRDX5 (PDB id: 2VL3) was docked into TLR4 receptor (PDB id: 3FXI) using ClusPro webserver (https://cluspro.bu.edu/login.php) (Kozakov et al., 2017) using custom settings. For each docking experiment, the ClusPro generated 20 most-probable docking poses. The most representative poses of the docking experiments are represented in Figures 5 and S5.

QUANTIFICATION AND STATISTICAL ANALYSIS

All experiments were performed in at least triplicate (n=3, experimental replication). For each experiment the number of replicate is provided in the figure caption. All data are expressed as the mean ± standard deviation (SD) and the differences between groups were compared using paired sample Student t-test. Significance is indicated within figures as *** signifying $p<0.001$.

DATA AND SOFTWARE AVAILABILITY

The software for the docking analysis is available under ClusPro webserver (https://cluspro.bu.edu/login.php).